Journal of Sound and Vibration (2002) **251**(1), 39–57
doi:10.1006/jsvi.2001.3977, available online at http://www.idealibrary.com on IDEAL®

FREE VIBRATIONS OF A RECTANGULAR PLATE CARRYING A DISTRIBUTED MASS

O. KOPMAZ AND S. TELLI

Department of Mechanical Engineering, College of Engineering and Architecture, Uludag University, Gorukle, Bursa 16059, Turkey,
E-mails: okopmaz@uludag.edu.tr; sevda@uludag.edu.tr

(*Received* 11 *December* 2000, *and in final form* 26 *July* 2001)

In this paper, an analytical method is presented to find the eigenfrequencies of a rectangular plate carrying a uniformly distributed mass. Using the standard Galerkin procedure, the equation of motion is reduced to a set of ordinary differential equations. From this set, the frequency equation is obtained. This polynomial equation is solved numerically. Due to the significance of the fundamental frequency of the system, its variation with respect to the non-dimensional parameters associated with the location, the area density and the distribution area of the mass attached to the plate, is investigated. Furthermore, it is shown by a numerical example that the method can be used to study plates with concentrated mass as a special case. Finally, an analysis to obtain the modal surfaces and the related nodal lines is carried out. It is demonstrated that the location of the attachment significantly affects the nodal lines, and modal interchanges may occur.

1. INTRODUCTION

Constrained flexible structures having several attachments are often encountered in engineering applications. Here, the word "constrained" takes place to emphasize that the plate, or the beam under study is equipped with some attachments that constrain the free vibrations of the structure. While there are publications on beams and rods with uniformly distributed mass [1–3], even if in a limited number, most literature about plates with attachments deals with plates carrying concentrated masses [4–7]. In this paper, the free transversal vibrations of a plate carrying distributed masses are investigated by means of a mathematical model. To discretize the derived partial differential equation the Galerkin procedure was utilized. Then, the eigenfrequencies and the eigenvectors of the system were obtained by using EIG that is a built-in function of Matlab®.

2. MODELLING AND EQUATIONS OF MOTION

Consider the system shown in Figure 1. The width, length and thickness of the plate are a, b and h respectively. Assume that the plate is isotropic. The plate thickness does not vary, and the plate is simply supported along all its edges. A distributed mass with dimensions c and d is located on the plate in the manner shown in Figure 1. The corner of the mass, closest to the origin is at point (x_0, y_0). Another significant assumption here is that the mass does not prevent the bending of the plate segment on which it is. In other words, the

0022-460X/02/110039 + 19 $35.00/0

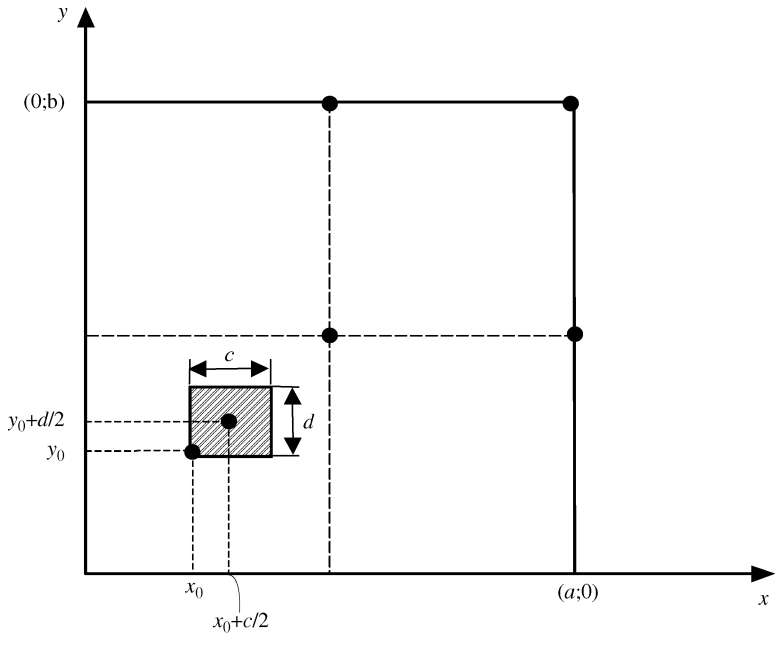

Figure 1. Plate with distributed mass.

attached mass can take the form of the plate region where it is located. As a consequence, it is possible to obtain the natural frequencies of a plate which has a distributed mass over its whole. In fact, this case corresponds to a uniform, unconstrained plate with a higher area mass density. Under these circumstances, the equation of motion of the plate is obtained as follows:

$$D\,(w_{xxxx} + 2\,w_{xxyy} + w_{yyyy}) + \bar{\rho}\,\ddot{w} = -\,\rho\,\ddot{w}\,\mathscr{H}(x, y, x_0, y_0, c, d), \tag{1}$$

where $w = w(x, y, t)$ represents the transverse deflection of the plate and lowercase letters x, y denote the partial derivatives with respect to x and y while the dots over w imply the time derivatives as usual. D is the flexural rigidity of the plate and is defined as

$$D = \frac{E\,h^3}{12\,(1\ -\ v^2)}, \tag{2}$$

where E, v and h are Young's modulus, the Poissons' ratio and the plate thickness respectively. Furthermore, $\bar{\rho}$ and ρ are the area density of the plate and the distributed mass respectively. Finally, the function $\mathscr{H}$ on the right-hand side of equation (1) is a combination of four Heaviside functions as follows:

$$\mathscr{H}(x, y, x_0, y_0, c, d) = [H(x - x_0) - H(x - x_0 - c)] \cdot [H(y - y_0) - H(y - y_0 - d)] \tag{3}$$

or

$$\begin{aligned}\mathscr{H}(x, y, x_0, y_0, c, d) = {} & \mathscr{H}_1(x - x_0, y - y_0) - \mathscr{H}_2(x - x_0, y - y_0 - d) \\ & - \mathscr{H}_3(x - x_0 - c, y - y_0) + \mathscr{H}_4(x - x_0 - c, y - y_0 - d).\end{aligned}$$

Note that the following relationships exist between the functions $\mathscr{H}_i$ and H:

$$\begin{aligned}
\mathscr{H}_1(x - x_0, y - y_0) &= H(x - x_0) \cdot H(y - y_0),\\
\mathscr{H}_2(x - x_0, y - y_0 - d) &= H(x - x_0) \cdot H(y - y_0 - d),\\
\mathscr{H}_3(x - x_0 - c, y - y_0) &= H(x - x_0 - c) \cdot H(y - y_0),\\
\mathscr{H}_4(x - x_0 - c, y - y_0 - d) &= H(x - x_0 - c) \cdot H(y - y_0 - d).
\end{aligned} \tag{4}$$

To apply the Galerkin discretization procedure to equation (1), the true solution of this equation is approximated with the following series:

$$w(x, y, t) = \sum_{i=1}^{N_x} \sum_{j=1}^{N_y} W_{ij}(x, y)\, q_{ij}(t), \tag{5}$$

where W_{ij} s are the modal functions of the unconstrained, simply-supported plate, and they are given as

$$W_{ij}(x, y) = \sin \frac{\mathrm{i}\pi x}{a} \sin \frac{\mathrm{j}\pi y}{b}. \tag{6}$$

Substituting equation (5) into equation (1), multiplying each term by $W_{rs}(x, y)$, and integrating all terms in the equation over the domain $(0 \leqslant x \leqslant a,\ 0 \leqslant y \leqslant b)$ gives:

$$\pi^4 \left[\left(\frac{r}{a}\right)^2 + \left(\frac{s}{b}\right)^2 \right]^2 D \frac{ab}{4} q_{rs} + \bar{\rho} \frac{ab}{4} \ddot{q}_{rs} + \rho ab \left[\sum_{i}^{N_x} \sum_{j}^{N_y} \bar{I}_{ij,rs}\, \ddot{q}_{ij} \right] = 0,$$

$$r = 1, \ldots, N_x \quad s = 1, \ldots, N_y. \tag{7}$$

After dividing each term by $\bar{\rho}ab/4$ and defining

$$\psi = \frac{b}{a}, \qquad \bar{\omega}_{rs} = \pi^2 [r^2 + (s/\psi)^2] \left(\frac{D}{\bar{\rho} a^4} \right)^{1/2} \tag{8, 9}$$

equation (7) takes the form

$$\ddot{q}_{rs} + \bar{\omega}_{rs}^2 q_{rs} + 4 \left(\frac{\rho}{\bar{\rho}} \right) \left[\sum_{i}^{N_x} \sum_{j}^{N_y} \bar{I}_{ij,\,rs}\, \ddot{q}_{ij} \right] = 0, \quad r = 1, \ldots, N_x, \quad s = 1, \ldots, N_y \tag{10}$$

where

$$\bar{I}_{ij,\,rs} = \begin{cases} = (\alpha_{11} - \alpha_{21})(\beta_{11} - \beta_{21}), & i \neq r, \quad j \neq s, \\ = (\alpha_{12} - \alpha_{22})(\beta_{11} - \beta_{21}), & i = r, \quad j \neq s, \\ = (\alpha_{12} - \alpha_{22})(\beta_{12} - \beta_{22}), & i = r, \quad j = s, \\ = (\alpha_{11} - \alpha_{21})(\beta_{12} - \beta_{22}), & i \neq r, \quad j = s, \end{cases} \tag{11}$$

$$\alpha_{11} = \frac{2}{(i^2 - r^2)\pi} (\mathrm{i} \cos \mathrm{i}\pi\xi \sin r\pi\xi - r \sin \mathrm{i}\pi\xi \cos r\pi\xi), \tag{12}$$

$$\alpha_{12} = \tfrac{1}{2}(1 - \xi) + \frac{1}{4r\pi} \sin 2r\pi\xi, \tag{13}$$

$$\alpha_{21} = \frac{2}{(i^2 - r^2)\pi}\left[\mathrm{i}\cos \mathrm{i}\pi(\xi + \gamma)\sin r\pi(\xi + \gamma) - r\sin \mathrm{i}\pi(\xi + \gamma)\cos r\pi(\xi + \gamma)\right], \tag{14}$$

$$\alpha_{22} = \tfrac{1}{2}(1 - \xi - \gamma) + \frac{1}{4r\pi}\sin 2r\pi(\xi + \gamma), \tag{15}$$

$$\beta_{11} = \frac{2}{(j^2 - s^2)\pi}(\mathrm{j}\cos \mathrm{j}\pi\zeta \sin s\pi\zeta - s\sin \mathrm{j}\pi\zeta \cos s\pi\zeta), \tag{16}$$

$$\beta_{12} = \frac{1}{2}(1 - \zeta) + \frac{1}{4s\pi}\sin 2s\pi\zeta, \tag{17}$$

$$\beta_{21} = \frac{2}{(j^2 - \mathrm{s}^2)\pi}[\mathrm{j}\cos \mathrm{j}\pi(\zeta + \delta)\sin s\pi(\zeta + \delta) - s\sin \mathrm{j}\pi(\zeta + \delta)\cos s\pi(\zeta + \delta)], \tag{18}$$

$$\beta_{22} = \frac{1}{2}(1 - \zeta - \delta) + \frac{1}{4s\pi}\sin 2s\pi(\zeta + \delta), \qquad \xi = \frac{x_0}{\mathrm{a}}, \qquad \zeta = \frac{y_0}{b}, \tag{19–21}$$

$$\gamma = \frac{c}{a}, \qquad \delta = \frac{d}{b}. \tag{22, 23}$$

δ_{ir} and δ_{js} in equation (10) are Cronecker deltas.

To reduce the indices in equation (10) the indices m and n are introduced and defined as

$$m = N_y(r - 1) + s, \quad i, r = 1, \ldots, N_x \tag{24}$$

$$n = N_y(i - 1) + j, \quad j, s = 1, \ldots, N_y \tag{25}$$

with $N = N_x N_y$, as m and n are taking integer values from 1 to N.

Then, equation (10) can be written in the following form:

$$\ddot{q}_m + \bar{\omega}_m^2 q_m + 4\left(\frac{\rho}{\bar{\rho}}\right)\left[\sum_{n=1}^{N} \bar{I}_{n,\,m}\ddot{q}_n\right] = 0, \quad m = 1, \ldots, N. \tag{26}$$

Substituting

$$\ddot{q}_n = -\omega^2 q_{\mathrm{n}} \tag{27}$$

into the set of equation (26) yields

$$\bar{\omega}_m^2 q_m - \sum_{n=1}^{N}\left[4\left(\frac{\rho}{\bar{\rho}}\right)\bar{I}_{n,m} + \delta_{nm}\right]\omega^2 q_n = 0, \quad m = 1, \ldots, N \tag{28}$$

or in the matrix form

$$[\bar{\boldsymbol{\omega}}^2]\{\mathbf{q}\} = \omega^2\,[[\mathbf{I}] + [\mathbf{Q}]]\,\{\mathbf{q}\} \tag{29}$$

where

$$[\bar{\boldsymbol{\omega}}^2] = \begin{bmatrix} \bar{\boldsymbol{\omega}}_1^2 & & & 0 \\ & \bar{\boldsymbol{\omega}}_2^2 & & \\ & & \ddots & \\ 0 & & & \bar{\boldsymbol{\omega}}_N^2 \end{bmatrix}. \tag{30}$$

$[\mathbf{Q}]$ is a matrix and its elements are

$$Q_{kl} = 4\left(\frac{\rho}{\bar{\rho}}\right)\bar{I}_{k,\,l} \tag{31}$$

and finally $[\mathbf{I}]$ is the unit matrix. Equation (29) can be rearranged as

$$\{\omega^2\{[\mathbf{I}] + [\mathbf{Q}]\} - [\bar{\boldsymbol{\omega}}^2]\}\{\mathbf{q}\} = \{0\}. \tag{32}$$

In order that equation (32) has non-trivial solutions, the determinant of the coefficients' matrix of the vector $\{\mathbf{q}\}$ must be equal to zero. Then, a polynominal in ω is found, the roots of which are the natural frequencies of the system. The explicit form of this characteristic determinant is as follows:

$$\begin{vmatrix} (1+Q_{11})\omega^2 - \bar{\boldsymbol{\omega}}_1^2 & Q_{12}\omega^2 & Q_{13}\omega^2 & \cdots & Q_{1,N}\omega^2 \\ Q_{21}\omega^2 & (1+Q_{22})\omega^2 - \bar{\boldsymbol{\omega}}_2^2 & Q_{23}\omega^2 & \cdots & Q_{2,N}\omega^2 \\ \vdots & & & & \\ \vdots & & & & \\ Q_{N,1}\omega^2 & Q_{N,2}\omega^2 & Q_{N,3}\omega^2 & \cdots & (1+Q_{N,N})\omega^2 - \bar{\boldsymbol{\omega}}_N^2 \end{vmatrix} = 0. \tag{33}$$

3. RESULTS

The natural frequencies of a rectangular plate that carries a distributed mass with its centre at $(x_0 + c/2, y_0 + d/2)$ were obtained by means of the method explained above. While doing this, the modes with which the frequencies are associated were not considered. Instead, all frequencies are arranged from the smallest to the greatest, and assessed in this manner.

Some non-dimensional parameters needed for calculations were chosen as:

$$\psi = \frac{b}{a} = 1{\cdot}5, \quad \gamma = \frac{c}{a} = 0{\cdot}1, \quad \delta = \frac{d}{b} = 0{\cdot}1,$$

$$\frac{\rho}{\bar{\rho}} = 10, \quad N_x = 5, \quad N_y = 5, \quad N = N_x N_y = 25.$$

The first 25 non-dimensional eigenfrequencies related to these modes of the unconstrained plate (i.e., the plate without carrying mass) are shown in Table 1. The eigenfrequencies were non-dimensionalized by multiplying by $(D/\bar{\rho}a^4)^{-1/2}$. In this table, the symbols in parentheses denote the associated modes. Since the plate has symmetry regarding its boundary conditions and geometry, it is concluded that the investigation on a quarter of the plate is sufficient for analysis purposes. Therefore, the values from 0·5 to 1 with the increments of 0·05 were assigned to the parameters ξ and ζ. For a certain pair of ξ and ζ values, the centre of the mass distributed on a rectangular region is located at $(\xi + \gamma/2, \zeta + \delta/2)$ in a non-dimensional form. The first 25 frequencies of the constrained plate are shown in Table 2 for $\xi = 0{\cdot}5\ (1{-}\gamma)$ and $\zeta = 0{\cdot}5(1 - \delta)$.

Since the fundamental frequency is the most significant for engineering applications, its variation with respect to the centre co-ordinates of the distributed mass was plotted by using three-dimensional graphical tools of Matlab®, (see Figure 2). Except for ξ and ζ, all the remaining parameters were kept constant in this analysis.

TABLE 1

The non-dimensional eigenfrequencies of a rectangular plate for $\psi = 1{\cdot}5$. The indices of the terms in the parentheses show the mode number associated with that frequency. Non-dimensionalizing factor: $(D/\bar{\rho}a^4)^{-1/2}$

$\omega_1 = (\omega_{11})$	14·2561	$\omega_{10} = (\omega_{24})$	109·6623	$\omega_{19} = (\omega_{44})$	228·0975
$\omega_2 = (\omega_{12})$	27·4156	$\omega_{11} = (\omega_{15})$	119·5319	$\omega_{20} = (\omega_{51})$	251·1266
$\omega_3 = (\omega_{21})$	43·8649	$\omega_{12} = (\omega_{33})$	128·3049	$\omega_{21} = (\omega_{52})$	264·2861
$\omega_4 = (\omega_{13})$	49·3480	$\omega_{13} = (\omega_{25})$	149·1407	$\omega_{22} = (\omega_{45})$	267·5759
$\omega_5 = (\omega_{22})$	57·0244	$\omega_{14} = (\omega_{34})$	159·0103	$\omega_{23} = (\omega_{53})$	286·2185
$\omega_6 = (\omega_{23})$	78·9568	$\omega_{15} = (\omega_{41})$	162·3002	$\omega_{24} = (\omega_{54})$	316·9240
$\omega_7 = (\omega_{14})$	80·0535	$\omega_{16} = (\omega_{42})$	175·4596	$\omega_{25} = (\omega_{55})$	356·4024
$\omega_8 = (\omega_{31})$	93·2129	$\omega_{17} = (\omega_{43})$	197·3921		
$\omega_9 = (\omega_{32})$	106·3724	$\omega_{18} = (\omega_{35})$	198·4887		

TABLE 2

The non-dimensional eigenfrequencies of a rectangular plate carrying a distributed mass with its centre at $(\xi + \gamma/2,\ \zeta + \delta/2)$ for $\psi = 1{\cdot}5,\ \gamma = \delta = 0{\cdot}1,\ \xi = 0{\cdot}5(1 - \gamma),\ \zeta = 0{\cdot}5(1 - \delta)$, $\rho/\bar{\rho} = 10$. Non-dimensionalizing factor: $(D/\bar{\rho}a^4)^{-1/2}$

ω_1	12·0092	ω_{10}	109·5762	ω_{19}	227·4303
ω_2	27·2403	ω_{11}	110·2799	ω_{20}	238·9339
ω_3	43·2103	ω_{12}	124·8148	ω_{21}	262·9828
ω_4	43·5832	ω_{13}	148·0554	ω_{22}	263·3200
ω_5	57·0125	ω_{14}	155·7927	ω_{23}	277·8061
ω_6	78·1580	ω_{15}	158·5821	ω_{24}	311·6927
ω_7	78·4819	ω_{16}	175·3214	ω_{25}	347·0318
ω_8	82·8148	ω_{17}	188·1630		
ω_9	105·7888	ω_{18}	193·6924		

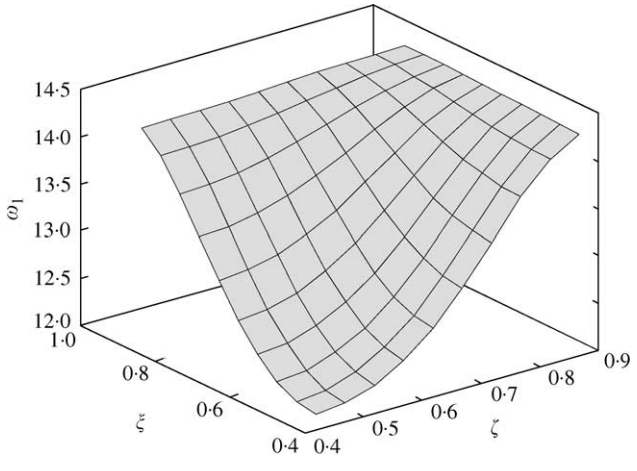

Figure 2. The variation of the first, non-dimensional eigenfrequency with respect to the corner position of the distributed mass. $\psi = 1{\cdot}5$, $\gamma = 0{\cdot}1$, $\delta = 0{\cdot}1$, $\rho/\bar{\rho} = 10$.

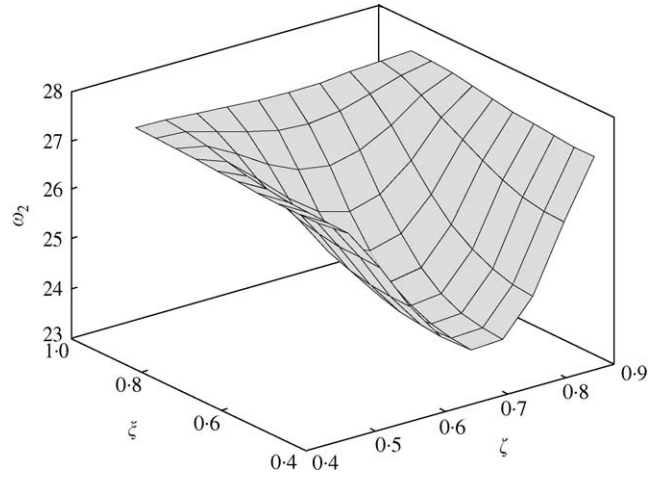

Figure 3. The variation of the second, non-dimensional frequency with respect to the corner position of the distributed mass. $\psi = 1{\cdot}5$, $\gamma = 0{\cdot}1$, $\delta = 0{\cdot}1$, $\rho/\bar{\rho} = 10$.

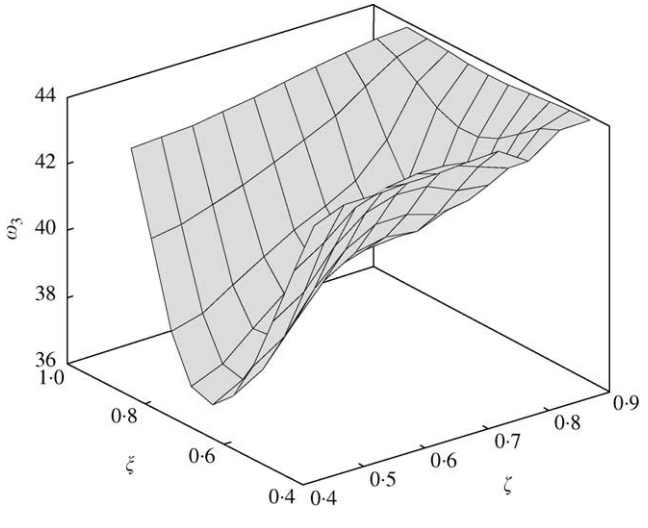

Figure 4. The variation of the third, non-dimensional frequency with respect to the corner position of the distributed mass. $\psi = 1{\cdot}5$, $\gamma = 0{\cdot}1$, $\delta = 0{\cdot}1$, $\rho/\bar{\rho} = 10$.

To indicate the effect of the mass location on the other frequencies (for example, the second and third ones), the similar graphics were also plotted (see Figures 3 and 4). The density ratio $\rho/\bar{\rho}$ appears to be another significant parameter worth investigating. As expected, the first eigenfrequency decreases as $\rho/\bar{\rho}$ is increased. Figures 5 and 6 show this phenomenon clearly for several $\rho/\bar{\rho}$ ratios of different order.

If the ratios γ and δ are made smaller while taking quite a large value for $\rho/\bar{\rho}$ also gives results for a plate carrying a concentrated mass. For instance, if $\delta = 0{\cdot}002$, $\gamma = 0{\cdot}002$ and $\rho/\bar{\rho} = 50\,000$ are chosen, gives the case of a plate carrying a lumped mass that weighs as one-fifth the plate mass. To make a comparison between the parameters of the plate and its attachment studied in reference [5] were used, and the first five eigenfrequencies were obtained. The frequencies found by the method given in reference [5] and by the exact

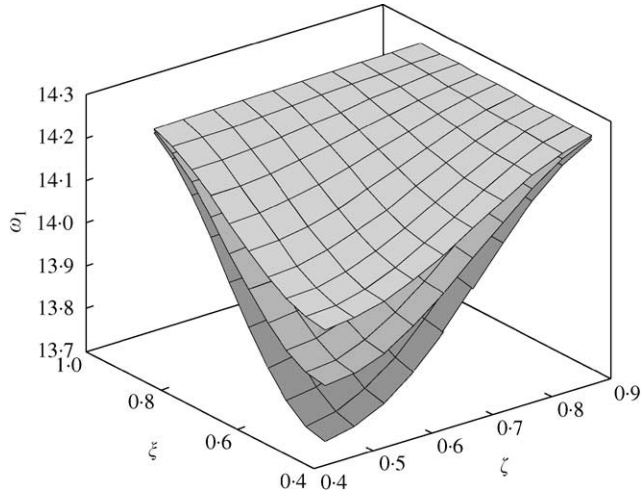

Figure 5. The variation of the first, non-dimensional frequency with respect to the corner position of the distributed mass for three different $\rho/\bar{\rho}$ ratios, from 1 to 2. $\psi = 1{\cdot}5$, $\gamma = 0{\cdot}1$, $\delta = 0{\cdot}1$: □, $\rho/\bar{\rho} = 1$; ■, $\rho/\bar{\rho} = 1{\cdot}5$; ■, $\rho/\bar{\rho} = 2$.

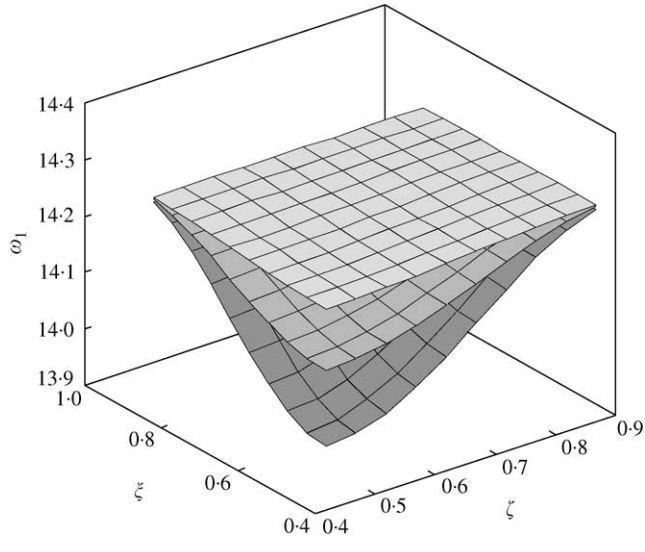

Figure 6. The variation of the first, non-dimensional frequency with respect to the corner position of the distributed mass for three different $\rho/\bar{\rho}$ ratios, from 0·1 to 1. $\psi = 1{\cdot}5$, $\gamma = 0{\cdot}1$, $\delta = 0{\cdot}1$: □, $\rho/\bar{\rho} = 0{\cdot}1$; ■, $\rho/\bar{\rho} = 0{\cdot}5$; ■, $\rho/\bar{\rho} = 1$.

solution are shown in Table 3. The comparison of the results indicates that the present approach is also appropriate for plates carrying concentrated masses.

As emphasized in section 2, the present model allows the frequencies of an unconstrained plate with higher area mass density to be found. For instance, when $\delta = \gamma = 1$ and $\rho/\bar{\rho} = 1$, the constrained system actually represents an unconstrained plate which has double the density of the constrained one. To verify the model for this special case, the frequencies of the plate for the above-mentioned parameters were computed. It was observed that these frequencies are in exact agreement with those obtained by equation (9).

TABLE 3

The first five eigenfrequencies for the example given in reference [5]. *The values in the first row were obtained by the present method* ($\psi = 1$, $\xi = 0{\cdot}25$, $\zeta = 0{\cdot}25$, $m_{attach} = 50$ kg)

	ω_1	ω_2	ω_3	ω_4	ω_5
The present method	31·7963	63·5739	95·4149	128·2167	181·0288
Reference [5]	31·8271	63·3374	95·4148	127·7677	180·6927
Exact solution	31·825	63·318	95·415	127·741	180·677

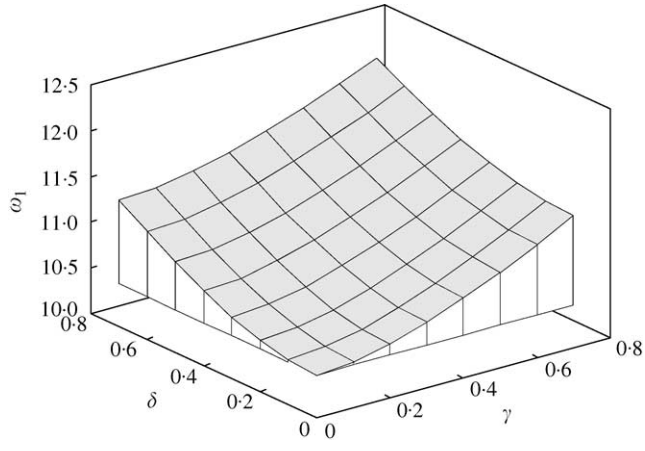

Figure 7. The variation of the first, non-dimensional frequency with respect to different mass dimensions. The parameters held constant are $\psi = 1{\cdot}5$, $m_{attachment}/m_{plate} = 0{\cdot}2$. (The mass centre of the attachment always coincides with the mass centre of the plate.)

The effect of varying the distribution area on the frequencies was also investigated. Holding the amount of the mass attached to the centre of the plate constant, the distribution area was changed assigning different values to γ and δ. Figure 7 shows the variation of the first frequency versus γ and δ. In Figure 8, the curves represent the variation of the first frequency versus the ratio of the mass distribution area to the plate area for constant γ and δ . These plots were obtained taking $\psi = 1{\cdot}5$, $m_{attachment}/m_{plate} = 0{\cdot}2$, $N = 25$. Although the results are not presented here, it was observed that the curves for constant and equal γ and δ values coincide for a square plate because of symmetry.

As known from vibrations theory when a linear elastic structure is excited in one of its natural frequencies its vibration approximates to the associated mode shape. Hence, an analysis to find modal surfaces and nodal lines (or nodes) of such a structure indicates where accurate devices like measurement instruments can be safely located on that structure. For this reason and in order to realize a complete analysis of the system considered in this work, the determination of the modal surfaces and the nodal lines of the constrained plate were also dealt with. A MATLAB code called EIG was utilized in finding the eigenvalues and the related approximate modal vectors **q** needed to form the modal surfaces. In this analysis, several cases were studied which can be grouped into two main categories. In the first group of studies, the attachment mass in a fixed position is altered and *vice versa* in the second group. The common factor in all these studies are the base area of the attachment and its mass. The distribution area is equal to one-hundreth of the plate area because $\delta = \gamma = 0{\cdot}1$.

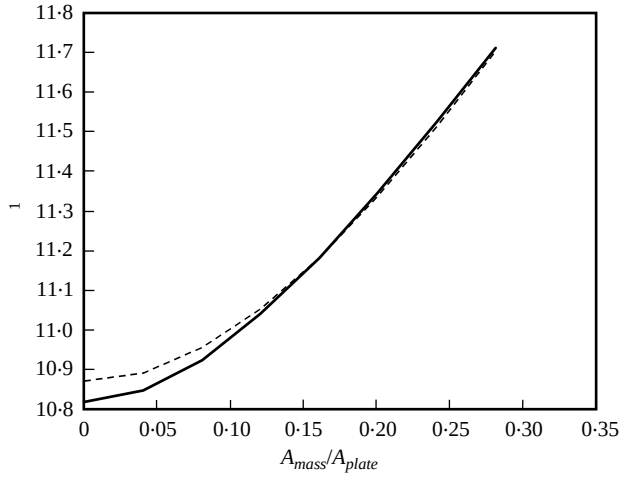

Figure 8. The first, non-dimensional frequency versus the area ratio (a) for constant γ , (b) for constant δ. The intersection point corresponds to the values $\gamma = \delta = 0{\cdot}4$. For this point, $A_{mass}/A_{plate} = 0{\cdot}16$: ——, γ: constant; – – – – –, δ: constant.

The attached mass is as much as 75% that of the plate, i.e., the ratio of the attached mass to that of the plate, the so-called mass ratio, equals to $\frac{3}{4}$. This is reached by assigning $\rho/\bar{\rho} = 0{\cdot}75 \times 10^2$ for the case of distributed mass. The distributed and concentrated mass loadings are also compared with each other. For the case of concentrated mass, it was assumed that $\delta = \gamma = 0{\cdot}01$ and $\rho/\bar{\rho} = 0{\cdot}75 \times 10^4$, so that this limiting case is approached very realistically. In all these analyses, the number of modes was taken as 25. Moreover, it was observed that there are no significant differences in the results when this number is 64. These case studies will now be presented and discussed.

Case Ia. A uniformly distributed mass is attached to the plate in such a manner that its centre of mass coincides with the geometric centre of the plate. As mentioned above, $\delta = \gamma = 0{\cdot}1$ and $\rho/\bar{\rho} = 0{\cdot}75 \times 10^2$. For this kind of loading, the first four modal surfaces are shown in Figures 9a, 9b, 9d and 9f. Figures 9c, 9e and 9g are the nodal lines maps for the second to fourth modes. There is no such map for the first mode because it has no nodal lines. Excepting the third one, the other modes remain the same as those of the unconstrained plate. It is also noticeable from the third modal surface, that the nodal line of third mode has an elliptic shape.

Case Ib. In this case, a concentrated mass is located at the centre of the plate instead of the distributed one. The modal surfaces and nodal maps will not be given here since they do not differ much from those of the distributed loading. However, the nodal line of elliptic shape related to the third mode has a smaller dimensions compared with the case of distributed loading. Note that for this case $\delta = \gamma = 0{\cdot}01$ and $\rho/\bar{\rho} = 0{\cdot}75 \times 10^4$.

Case IIa. The distributed mass is located at the centre of the quarter plate. The density ratio and the attachment dimensions are the same as those in Case Ia. The first four modal surfaces and their nodal line maps related to this case are seen in Figure 10. Here, it is easily seen that the nodal lines differ remarkably from those of the unconstrained plate.

Case IIb. In this case, there is a concentrated mass of the same amount as that of the distributed one. All the modal surfaces are almost similar to those of the distributed loading case. Only in the fourth nodal lines map, a relatively small difference from the fourth map in Case IIa given in Figure 10(g) is observed as shown in Figure 11(b) while the modal surfaces appear the same when compared with Figures 10(f) and 11(a). Only the fourth nodal lines

map has a relatively small difference from its counterpart in Case IIa as is easily seen from comparison of Figure 11(b) with Figure 10(g) while the associated modal surfaces have the same appearance (Figures 10(f) and 11(a)).

Case III. This case study is a kind of generalization of those presented and explained above. In this analysis, a distributed mass having the parameters already given is located at several points in three different directions, namely, starting from the geometric centre of the plate, parallel to the long edge (y-axis), parallel to the short edge (x-axis) and on the diagonal of the top right (according to the co-ordinate system defined in this work) quarter plate. The results of these subcases which will be called IIIa, IIIb and IIIc are as follows:

Case IIIa. A distributed mass loading was assumed to be applied at five points spaced at equal distances on a straight line connecting the plate centre and the midpoint of the (top) short edge, respectively, and for each loading, the second to fourth nodal maps were plotted. During this case study, ξ is fixed and equal to 0·45 while ζ take the values 0·45, 0·5625, 0·6750, 0·7875 and 0·90 respectively. In Figures 12(a–c), the variation of the nodal lines with the locations of the attachment is shown. Due to the geometry of the problem, all the lines are symmetric with respect to the direction on which the loadings are applied. The nodal

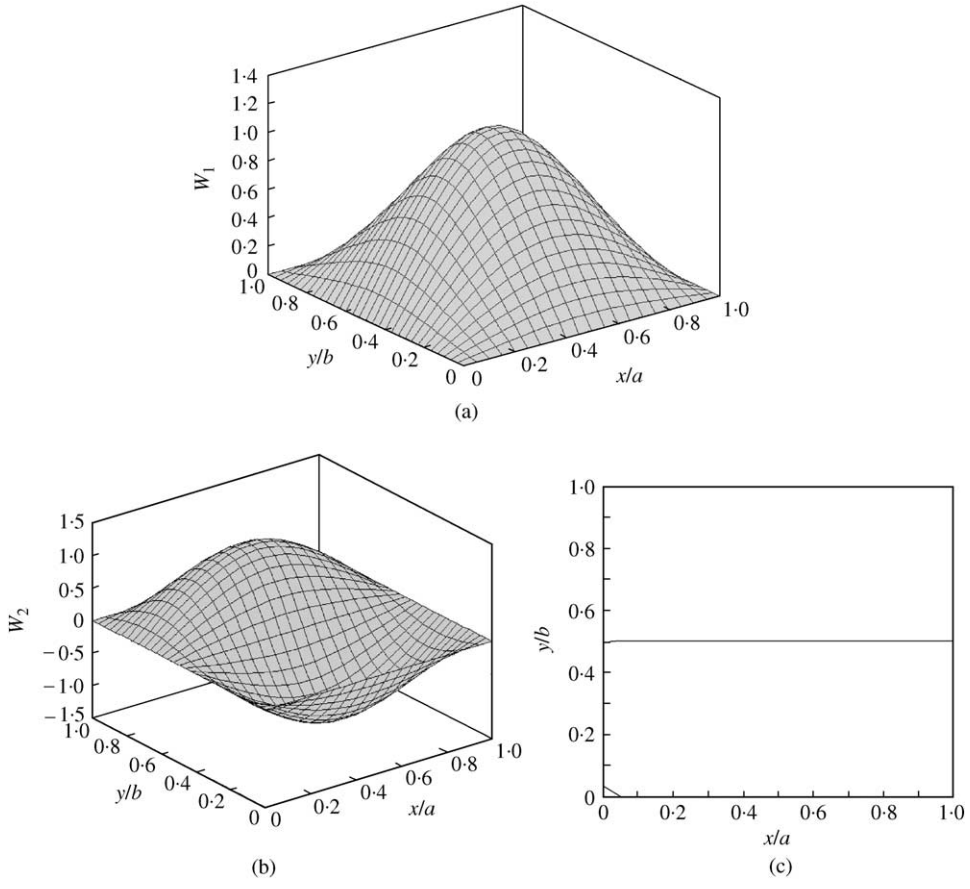

Figure 9. Modal surfaces and nodal lines of constrained plate for distributed mass loading. $\delta = \gamma = 0{\cdot}1$, $\rho/\bar{\rho} = 0{\cdot}75 \times 10^2$ ($m_{attachment}/m_{plate} = 3/4$), $\xi = \zeta = 0{\cdot}45$ (the attachment is at the plate centre): (a) first modal surface; (b) second modal surface; (c) second nodal lines map; (d) third modal surface; (e) third nodal lines map; (f) fourth modal surface; (g) fourth nodal lines map.

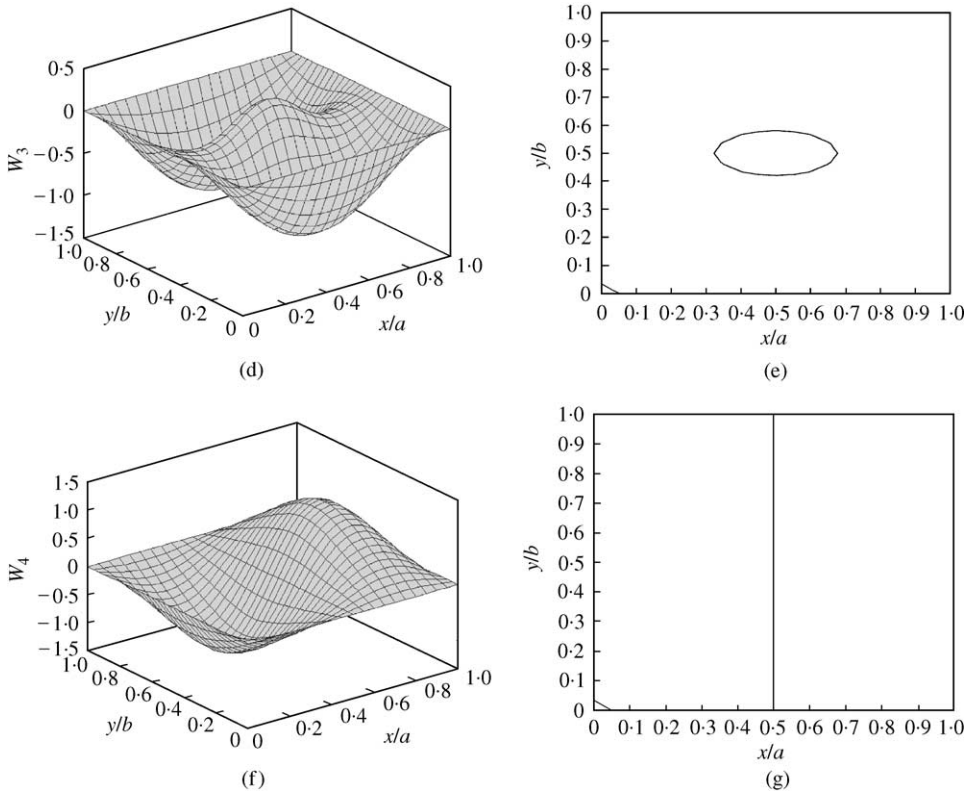

Figure 9. Continued.

line of the second mode moves first in the $+y$ direction, but when the centre of distributed mass is very close to or on the short edge, it starts coming back to the centre of the plate (Figure 12(a)). In the third mode, when the mass moves towards the short edge, the elliptic nodal line is replaced with two nodal lines (i.e., in other words, a two parted nodal line). For $\zeta = 0{\cdot}6750$, the nodal line consists of a vertical straight line as shown in Figure 12(b). When ζ increases the nodal line again separates into two different lines.

The nodal map of the fourth mode has a vertical straight line for central mass loading. When the centre of the attachment is at point (0·50;0·6125), this mode has two nodal lines. As the mass continues moving towards the top in the $+y$ direction, for all other positions of the attachment, the nodal lines consist of a vertical straight line and are coincident with each other (Figure 12(c)).

Case IIIb. In this case, the distributed mass is moved in the $+x$ direction starting from the centre of the plate. Similar to the previous case, due to structural and geometric symmetry, the nodal lines are also symmetric with respect to the straight line connecting the midpoints of the long edges. In this analysis ζ is held constant and equals 0·45 as ξ takes the values 0·45, 0·5625, 0·6750, 0·7875 and 0·90. (Note that to find the co-ordinates of the attachment centre, 0·05 should be added to the values ζ and ξ). For the second mode, the unique difference in nodal lines occurs for $\xi = 0{\cdot}7875$. For other loadings, the nodal lines consists of the symmetry axis of the plate, parallel to the x-axis, (Figure 13(a)).

In the third mode, the originally elliptic nodal line converts to semi-ellipses when ξ increased, but it comes back, expanding towards the plate centre when $\xi = 0{\cdot}90$. The

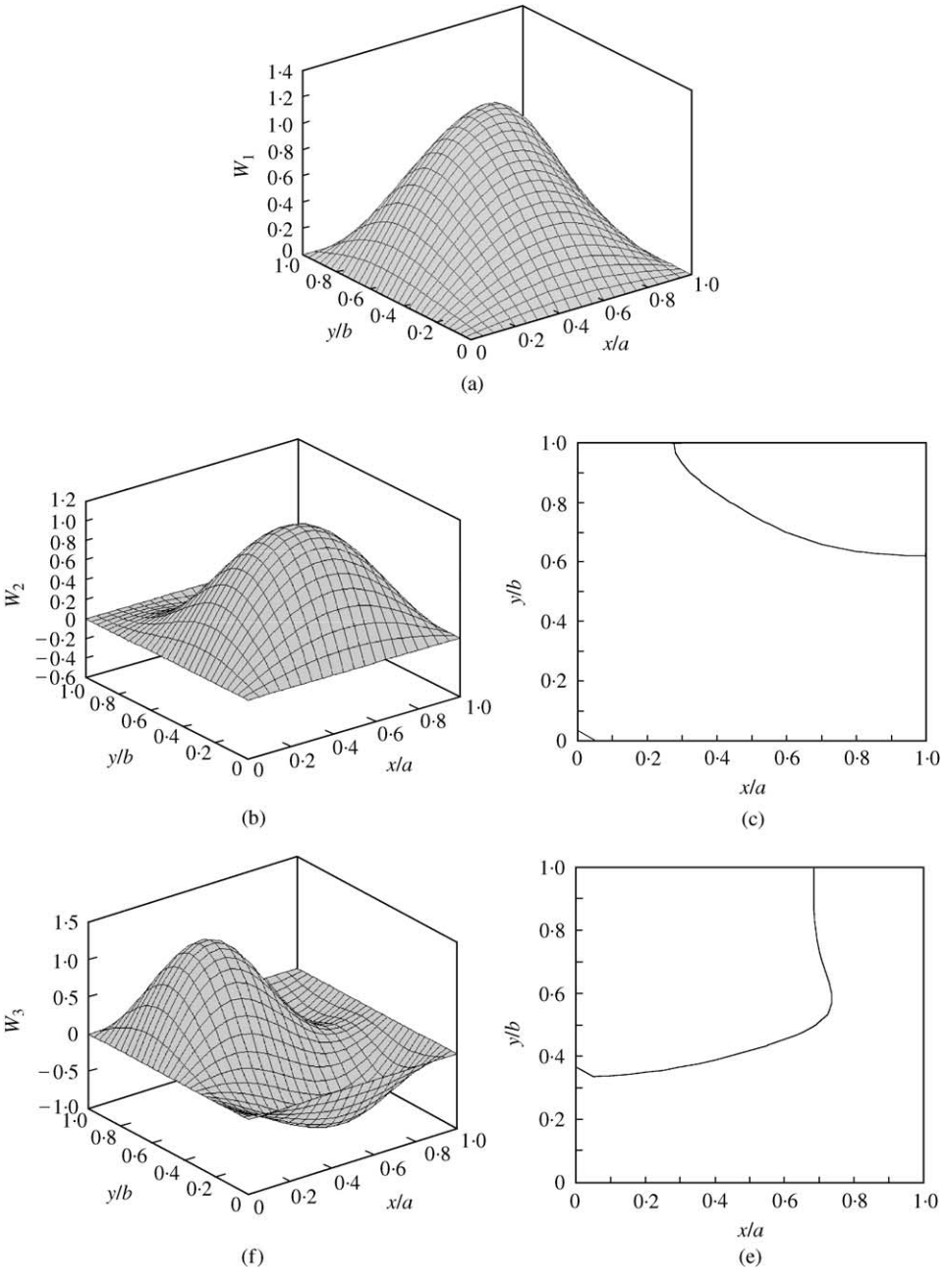

Figure 10. Modal surfaces and nodal lines of constrained plate for distributed mass loading. $\delta = \gamma = 0{\cdot}1$, $\rho/\bar{\rho} = 0{\cdot}75 \times 10^2$ ($m_{attachment}/m_{plate} = 3/4$), $\xi = \zeta = 0{\cdot}6750$ (the attachment is at the centre of the quarter plate): (a) first modal surface; (b) second modal surface; (c) second nodal lines map; (d) third modal surface; (e) third nodal lines map.

fourth mode is more interesting regarding its nodal lines. In this mode, the nodal line that is originally a straight line is replaced with semi-ellipses (Figure 13(b)). Regarding the fourth mode, the nodal line is a straight line for loading at $\xi = 0{\cdot}45$. For intermediate positions of the attachment the nodal lines are semi-ellipses which become flatter. When the mass is very

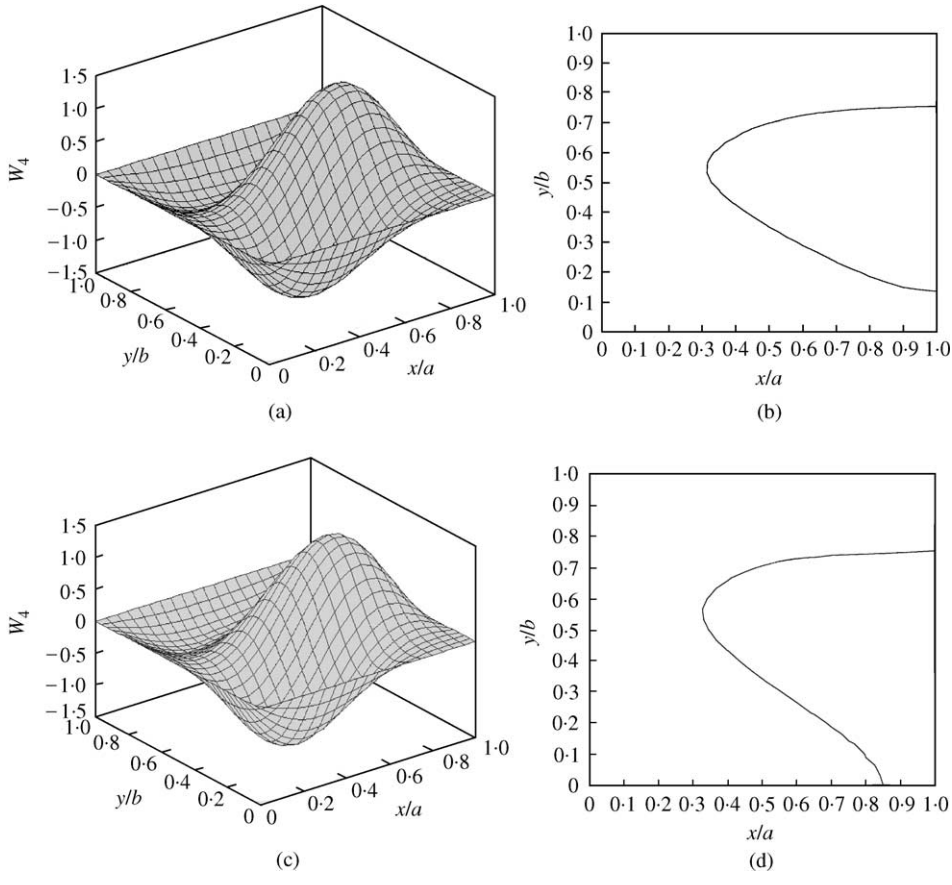

Figure 11. Fourth modal surfaces and nodal lines for distributed and concentrated mass loading, respectively. $m_{attachment}/m_{plate} = 3/4$, $\xi = \zeta = 0{\cdot}6750$ (the attachment is at the centre of the quarter plate): (a) modal surface for distributed loading. $\delta = \gamma = 0{\cdot}1$, $\rho/\bar{\rho} = 0{\cdot}75 \times 10^2$; (b) nodal map for distributed loading; (c) modal surface for concentrated loading. $\delta = \gamma = 0{\cdot}01$, $\rho/\bar{\rho} = 0{\cdot}75 \times 10^4$; (d) nodal map for concentrated loading.

close or partly on the long edge, two parted nodal lines take the place of the semi-ellipses (Figure 13(c)).

Case IIIc. During this analysis, the attached mass is moved on the diagonal connecting the centre and corner points of the plate (the points (0·5,0·5) and (1,1) in the non-dimensional form and (a/2,b/2) and (a,b) in the dimensional form). The nodal line of the second mode that is a horizontal straight line at the beginning, initially becomes concave towards the corner point but when $\xi = \zeta = 0{\cdot}9$, it returns back to its original position (Figure 14(a)). In the third mode, the nodal line follows a quite complicated pattern. For the intermediate values of ξ and ζ, the nodal line becomes two parted, and when the centre of the attachment is very close or at the corner point, the nodal line is again a one-parted curve (Figure 14(b)).

For the loading at the plate centre, the nodal line of the fourth mode is a straight line parallel to the y-axis. Also in this mode, the variation of nodal lines develop in a quite complicated manner. What is noticeable here is that a two-parted nodal line appears when the attachment approaches the corner (Figure 14(c)). Note that the symmetry of nodal lines is lost.

Case IV. This final case study was carried out to determine how different distributed mass loadings affect the nodal lines of the plate provided that the attachment is located at the

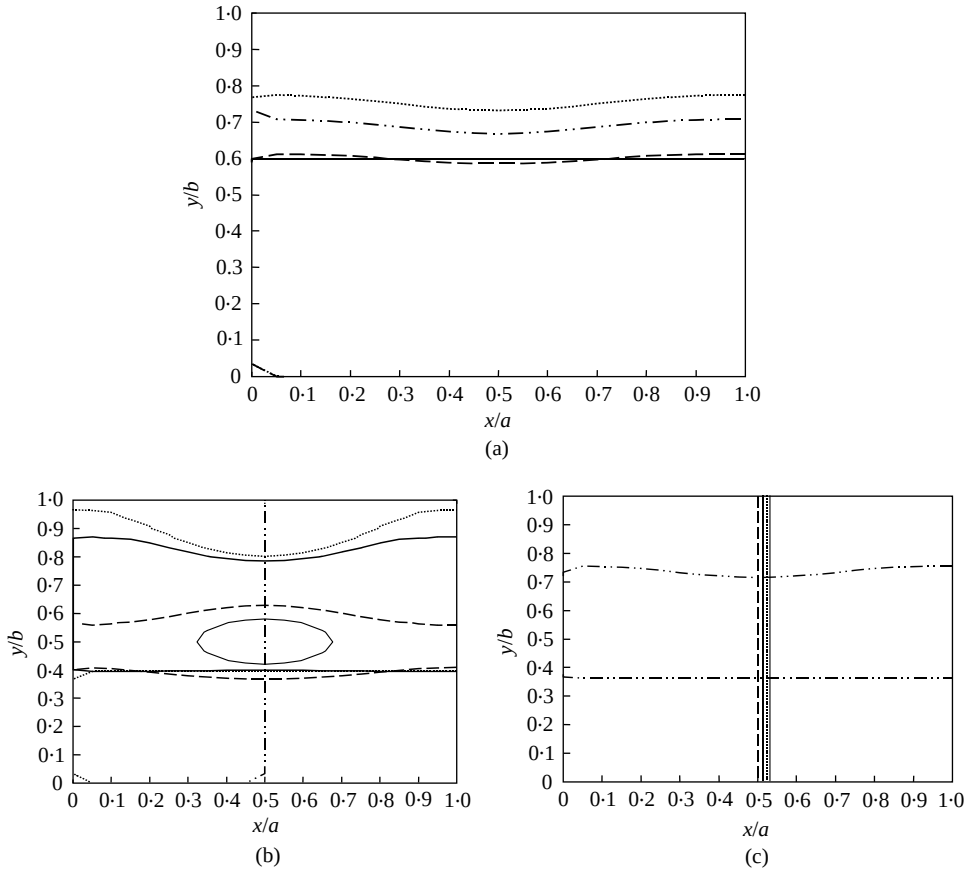

Figure 12. Variations of nodal lines when the attachment displaces in the direction parallel to the long edge. $\delta = \gamma = 0{\cdot}1$, $\rho/\bar{\rho} = 0{\cdot}75 \times 10^2$ ($m_{attachment}/m_{plate} = 3/4$), $\xi = 0{\cdot}45$. ———, $\zeta = 0{\cdot}45$; – – – –, $\zeta = 0{\cdot}5625$; – · – · –, $\zeta = 0{\cdot}6750$; ·····, $\zeta = 0{\cdot}7875$; ———, $\zeta = 0{\cdot}90$. (a) second nodal lines map; (b) third nodal lines map; (c) fourth nodal lines map (Note that all straight lines are coinciding with each other in Figure 12(c)).

centre of the quarter plate. Figures 15(a), 15(c) and 15(e), shows the nodal lines of the unconstrained plate. Figures 15(b), 15(d), and 15(f) show the variation of nodal lines of the second to fourth modes for different mass loadings. From the comparison of these figures, it is concluded at first glance that the location and mass of an attachment seriously affect the nodal lines of a plate. Another observation worth mentioning is an interchange of nodal lines between the third and fourth modes, as can be seen in Figure 15(d) and 15(f).

At this point, it should be noted that the mass ratio cannot be selected as large as desired because the linear Euler–Bernoulli hypothesis may be violated, or the plate material may have reached its yield point. To illustrate this, a static analysis with dimensional quantities was carried out to obtain the static deflections and slopes of the plate for the above-mentioned mass ratios. For this analysis, the physical parameters and dimensions of the plate were taken as $E = 2{\cdot}1 \times 10^{11}$ N/m^2 (steel), $a = 2$ m, $b = 3$ m, (hence, $\psi = b/a = 1{\cdot}5$), $h = 0{\cdot}005$, $m = 5$ mm (thickness), ρ_v (volumetric density) $= 7850$ kg/m^3, $\bar{\rho} = 39{\cdot}25$ kg/m^2 ($= \rho_v h$ for a uniform plate). Since the largest deflection for the attached mass of any amount is expected to occur at the geometric centre of the plate when the mass loading is applied at that point, it was assumed that the attachment is located there. First,

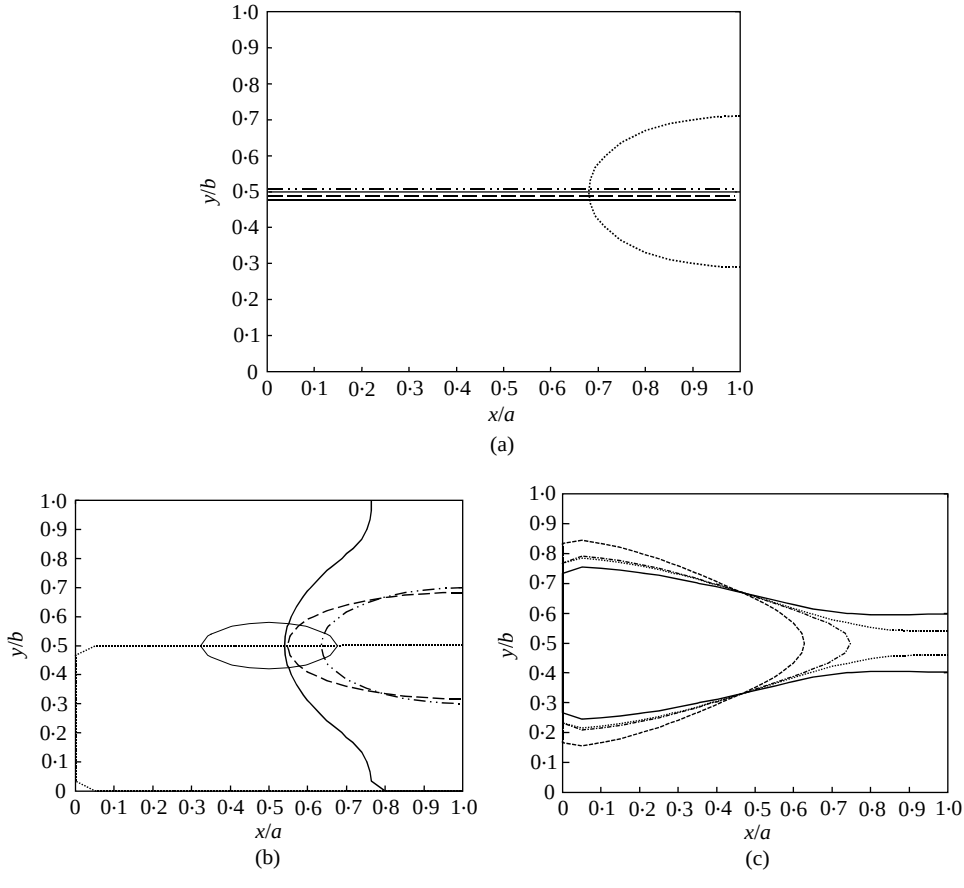

Figure 13. Variations of nodal lines when the attachment displaces in the direction parallel to the short edge. $\delta = \gamma = 0{\cdot}1$, $\rho/\bar{\rho} = 0{\cdot}75 \times 10^2$ ($m_{attachment}/m_{plate} = 3/4$), $\zeta = 0{\cdot}45$; ————, $\xi = 0{\cdot}45$; – – – – –, $\xi = 0{\cdot}5625$; – ·· – –··, $\xi = 0{\cdot}6750$; ·····, $\xi = 0{\cdot}7875$; ————, $\xi = 0{\cdot}90$. (a) second nodal lines map (Note that all straight lines are coinciding with each other in Figure 13(a); (b) third nodal lines map; (c) fourth nodal lines map.

the maximum static deflection and slope of the plate due to its own weight was found. Then, the same process was continued considering just the attachment weights. It was observed that for the mass ratios equal to and greater than 4, the linear Euler–Bernoulli hypothesis loses its validity with regard to the total maximum plate slope as seen in Table 4. Therefore, when the present method is used for such an analysis, a preliminary investigation on the validity of the linear bending theory is necessary and useful. The results of this static analysis are presented in Table 4. For the central loading described above, the maximum slope arises at the midpoint of the long edge in the x direction, i.e., in the direction parallel to the short edge.

4. CONCLUSIONS

In this work, the free vibrations of a plate carrying a distributed mass was investigated. A mathematical procedure was developed based on the Galerkin method, and using this non-dimensionalized procedure the eigenfrequencies of a constrained plate were obtained.

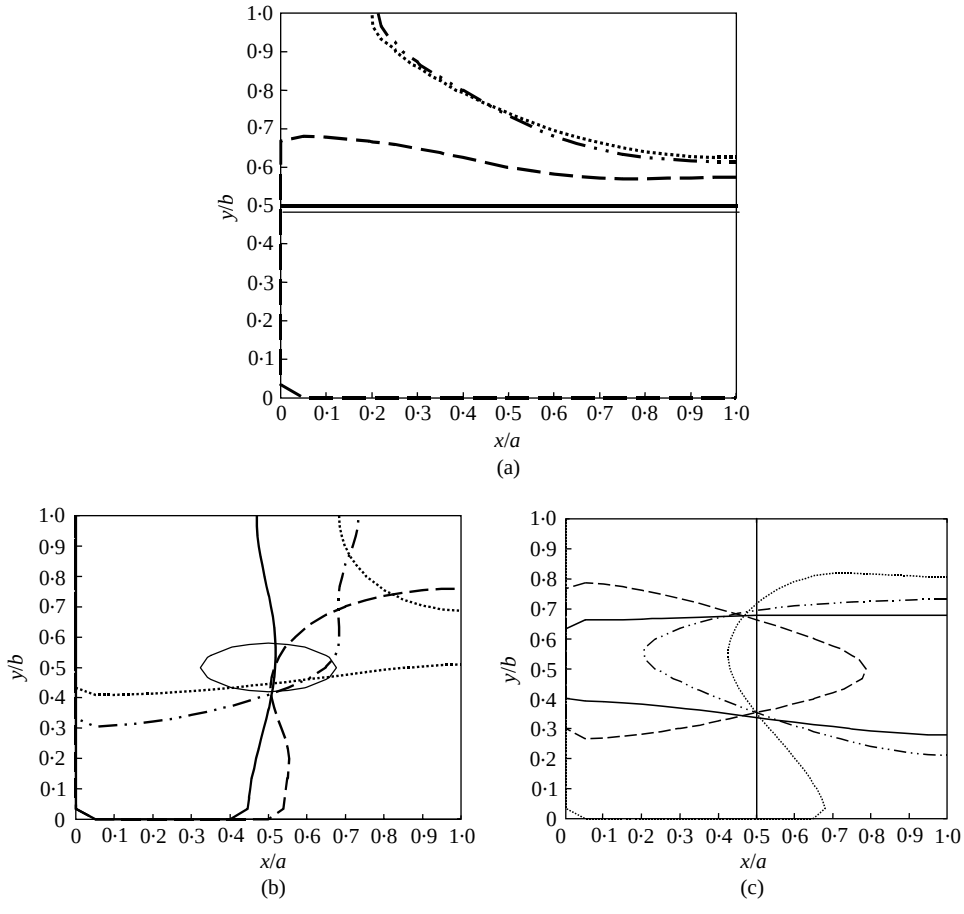

Figure 14. Variations of nodal lines when the attachment displaces on the diagonal of the quarter plate. $\delta = \gamma = 0{\cdot}1$, $\rho/\bar{\rho} = 0{\cdot}75 \times 10^2$ $(m_{attachment}/m_{plate} = 3/4)$. ————, $\xi = \zeta = 0{\cdot}45$; – – – –, $\xi = \zeta = 0{\cdot}5625$; —··—··—, $\xi = \zeta = 0{\cdot}6750$; ·····, $\xi = \zeta = 0{\cdot}7875$; ————, $\xi = \zeta = 0{\cdot}90$. (a) second nodal lines map; (b) third nodal lines map; (c) fourth nodal lines map.

TABLE 4

The results of static analysis

$\frac{m_{attachment}}{m_{plate}}$	Total maximum deflection (m) $x = a/2$ $y = b/2$	Total *maximum slope* (°) $x = 0(= a)$ $y = b/2$
0	0·0202	1·8793
1	0·0789	6·4973
2	0·1376	11·1097
3	0·1963	15·7277
4	0·2549	20·3400
5	0·3136	24·9580

The effect of some non-dimensional parameters such as the density ratio, the distribution area ratio, on the frequencies was also investigated. Furthermore, it was shown that this method enables one to study plates carrying concentrated (lumped) mass. An important

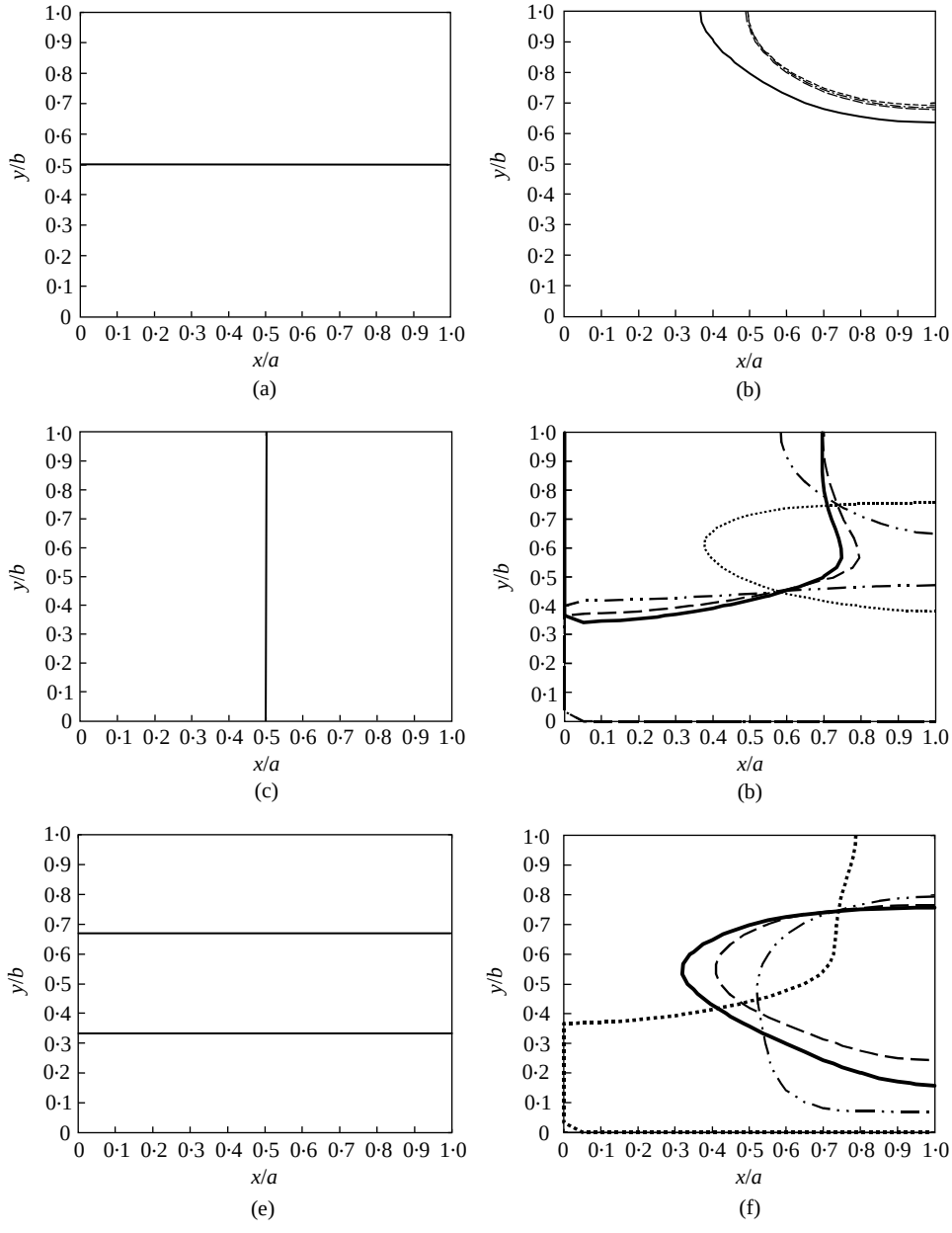

Figure 15. Variation of nodal lines for different mass loadings. (a), (c) and (e) Nodal lines for the second, third and fourth modes at the unconstrained plate respectively. (b), (d) and (f) Nodal lines for the second, third and fourth modes at the constrained plate for different mass loading respectively. The attachment is at the centre of the quarter plate. $\delta = \gamma = 0{\cdot}1$. ————, $m_{attachment}/m_{plate} = 1$; – – – –, $m_{attachment}/m_{plate} = 3$; – – · · – –, $m_{attachment}/m_{plate} = 4$, ·····, $m_{attachment}/m_{plate} = 5$.

conclusion drawn from this study is that the frequencies of a plate as a structural element may be changed by locating the attached mass (it usually represents the mass of a machine mounted on the floor that can be considered as a plate) in such a manner that the frequency of the machine excitation is far away from those of the plate.

For the completeness of the present study, the modal surfaces and the associated nodal lines of the constrained plate considered here were also obtained. Two important results, reached by this analysis, are that an interchange between nodal lines may occur when the amount of the attached mass is increased, and for the second to fourth modes which are practically relevant, the nodal lines move back towards to the inside region of the plate when the attachment stays very close to or is partly located on the edges of the plate.

REFERENCES

1. K.-T. CHAN, X.-Q. WANG and T.-P. LEUNG 1998 *Journal of Vibration and Acoustics* **120**, 944–948. Free vibration of beams with two sections of distributed mass.
2. K.-T. CHAN and J.-Z. ZHANG 1995 *Journal of Sound and Vibration* **182**, 185–190. Free vibration of a cantilever tube partially filled with liquid.
3. K.-T. CHAN, T.-P. LEUNG and W.O. WONG 1996 *Journal of Sound and Vibration* **191**, 590–597. Free vibration of simply supported beam partially loaded with distributed mass.
4. R. E. ROSSI and P. A. A. LAURA 1996 *Journal of Sound and Vibration* **195**, 142–148. Symmetric and antisymmetric normal modes of a cantilever rectangular plate: effect of Poisson's ratio and a concentrated mass.
5. J.-S. WU and S.-S. LUO 1997 *Journal of Sound and Vibration* **200**, 179–194. Use of the analytical and numerical combined method in the free vibration analysis of a rectangular plate with any number of point masses and translational springs.
6. P. D. CHA 1997 *Journal of Sound and Vibration* **207**, 593–596. Free vibration of a rectangular plate carrying a concentrated mass.
7. K.-T. CHAN and X.-Q. WANG 1997 *Journal of Sound and Vibration* **206**, 353–369. Free vibration of a Timoshenko beam partially loaded with distributed mass.